Synthesis and characterization of plate-like vanadium doped SrBi$_4$Ti$_4$O$_{15}$ prepared via KCl molten salt method

Puspa Sari[a], Suci Noerfaiqotul Himmah[a], Arie Hardian[b], Nur Aini[a], Anton Prasetyo[a,*]

[a]*Department of Chemistry, Faculty of Sciences and Technology, Universitas Islam Negeri Maulana Malik Ibrahim Malang, Malang 65144, Indonesia*
[b]*Department of Chemistry, Faculty of Sciences and Informatics, Universitas Jenderal Achmad Yani, Cimahi 40531, Indonesia*

Abstract

SrBi$_4$Ti$_4$O$_{15}$ is one of the four-layered Aurivillius compounds that can be used as photocatalyst material. Expanding its work function under a wider wavelength can be conducted by introducing a metal dopant into SrBi$_4$Ti$_4$O$_{15}$ in view of its reduced band gap energy. In this research, vanadium doped SrBi$_4$Ti$_4$O$_{15}$ (SrBi$_4$Ti$_{4-n}$V$_n$O$_{15}$ (n= 0, 0.05, 0.1, and 0.15)) was synthesized via molten KCl salt method. The diffractogram showed that the SrBi$_4$Ti$_{4-n}$V$_n$O$_{15}$ compounds (n= 0, 0.05, 0.1, and 0.15) were successfully crystallized in space group $A2_1am$ without any impurities. The SEM micrographs confirmed the plate-like morphology of SrBi$_4$Ti$_{4-n}$V$_n$O$_{15}$ (n= 0, 0.05, 0.1, and 0.15) and the calculation of the Kubelka-Munk function on the UV-Vis DRS spectra showed that the vanadium effectively reduced the band gap energy value from 3.04 eV (408 nm) to 2.84 eV (437 nm).

Keywords: SrBi$_4$Ti$_4$O$_{15}$; V dopant; molten salt method; KCl

1. Introduction

The photocatalyst properties of Aurivillius compounds have attracted many researchers for further investigation [1-4]. It is due to the ferroelectric properties of the Aurivillius compound, which can inhibit the electron and hole recombination [5], thus enabling them to enhance the lifetime of reduction–oxidation reaction. The favorable photocatalytic activity of Aurivillius compounds have been widely reported for dyes waste treatment such as rhodamine-B (RhB), methyl orange (MO), and methylene blue (MB) [2-3, 6].

Aurivillius compound is composed alternately between (Bi$_2$O$_2$)$^{2+}$ layer and pseudo-perovskite ($A_{m-1}B_m$O$_{3m+1}$)$^{2-}$ layer along the c-axis [7]. Whereas, the m denotation represents the number of pseudo-perovskite layers. A-cation consists of the larger cation with low valences, such as Bi, Ba, Sr, Ca, Na, K, Pb, or rare earth metals. In comparison, B-cation consists of the smaller cation with high valences, such as Ti, W, Fe, Ta, Nb, and Mo, which occupy the center of oxygen octahedral [8]

A well-known strategy to reduce the band gap energy is by doping photocatalyst compounds with a metal element such as vanadium (V). Typically, it is due to the similarity of ionic radii between Ti and V that will facilitate the doping process [9]. Using V as doping can form some new electronic transitions to reduce its band gap energy [10-12]. Kamegawa, et al. synthesized the V-doped TiO$_2$ and suggested that the addition of V dopant could shift light absorption towards a larger

wavelength >380 nm due to the creation of impurity energy levels in the TiO$_2$ band gap [13]. Meanwhile, Bantawal, et al. synthesized V-doped SrTiO$_3$ and reported that V dopants effectively reduced the band gap energy of SrTiO$_3$ from 3.16 to 2.13 eV. They suggested that this was due to the substitution of V into Ti^{4+} lattice resulting in a defect of mixing V-d with Ti-d orbitals in the conduction band to create a persistent band that extended downward and induced to reduce the band gap energy [14].

Many researchers have reported the utilization of vanadium doped Aurivillius photocatalyst compounds. For instance, Gu, et al. synthesized vanadium doped Bi$_4$Ti$_3$O$_{12}$ and reported that vanadium dopant could reduce its band gap energy value and caused a shift of light absorption towards visible light as a result of the contribution of V 3d orbitals in the conduction band [15]. It indicated that vanadium doping had a potential to reduce the bandgap energy of other Aurivillius compounds. SrBi$_4$Ti$_4$O$_{15}$ is one of the four-layered Aurivillius compound family members, which is reported to have photocatalytic properties with band gap energy of 3.0 eV (λ= 413 nm or violet light range) [5]. Reducing the band gap energy from SrBi$_4$Ti$_4$O$_{15}$ can provide some benefits related to its utilization as a photocatalyst compound. Based on the above description, V has the potential to be used as a doping of SrBi$_4$Ti$_3$O$_{15}$ to decrease the band gap energy value. Zhu, et al. synthesized the V-doped SrBi$_4$Ti$_4$O$_{15}$ using solid state reaction method, and reported that it could enhance to its ferroelectric properties [16]. However, the effects of V dopant on SrBi$_4$Ti$_4$O$_{15}$ band gap energy, so far, has not been reported yet. On the other hand, one of the disadvantages of solid-state reaction method is the

agglomeration formed on sample produce due to the higher temperature conditions of synthesis.

Another factor affecting photocatalyst activity are particle size and morphology [17]. The plate-like/sheet Aurivillius compound has been reported to have good photocatalyst properties [18]. Jakhade, et al. synthesized Bi_2WO_6 and obtained the different morphology i.e. nanoplates and nanoflakes arranged like a rose and reported that the morphology particle of photocatalyst material affected its photocatalytic activity in which nanoflake Bi_2WO_6 had a better photocatalytic activity [19]. Meanwhile, Jiang et al. synthesized $Bi_4Ti_3O_{12}$ nanosheets and reported that it could degrade RhB by 40% in 90 minutes [20]. Another work also reported by Cheng, et al. that synthesized $Bi_4Ti_3O_{12}$ using the hydrothermal method with the addition of tert-butylamine as well as oleic acid to modify the particle morphology. They obtained two types of morphology i.e. (a) microspheres and (b) microrods and reported that microrods particles showed the best degradation activity [21]. In addition, Sreeram, et al. reported that indium vanadium material in sheet morphology exhibited a good photocatalyst activity [22].

Molten salt method is a synthesis method widely reported in producing oxide metal with its typical morphology as well as without any agglomeration formed. In this method, salt is mixed to precursors and heated over the melting point of salt, so the molten salt works as a reaction medium [23-25]. The molten salt method has many advantages such as simple method, the relatively low calcination temperature required to create a pure product, and high homogeneity and good crystallinity of the product. This method can also control particles' size as well as shape and reduce particles' agglomeration [26, 27].

The use of the molten salt method to synthesize plate-like/sheet Aurivillius compounds has been reported by many researchers. Zhao et al. synthesized $Bi_4Ti_3O_{12}$ photocatalyst using the molten salt method and successfully obtained plate-like $Bi_4Ti_3O_{12}$. They also reported that $Bi_4Ti_3O_{12}$ could degrade 90% MB for 120 minutes [28]. He et al. synthesized $Bi_4Ti_3O_{12}$ using the solid-state reaction (SSR) and the molten salt method and successfully obtained $Bi_4Ti_3O_{12}$. However, this resulted in some differences in particle morphology. The SSR method produces some particles with irregular morphology, while the molten salt method produces a plate-like morphology that has a better photocatalytic activity [29]. It indicates that the molten salt method has some advantages in synthesizing photocatalyst materials. Therefore, in this research, V-doped $SrBi_4Ti_4O_{15}$ ($SrBi_4Ti_{4-n}V_nO_{15}$ (n= 0, 0.05, 0.1; and 0.15) was synthesized by molten salt method (used KCl salt) with an aim to reduce the band gap energy of $SrBi_4Ti_4O_{15}$.

2. Materials and Methods

2.1. Precursor

The precursors used in this research included Bi_2O_3 (Sigma-Aldrich, 99.9%), $SrCO_3$ (Sigma-Aldrich, 99.9%), V_2O_5 (Sigma-Aldrich, 99.9%), TiO_2 (Sigma-Aldrich, 99.9%), KCl (Merck 99%), $AgNO_3$ (Merck, 99.9%), and acetone (Merck).

2.2. Synthesis and characterization

All precursors (Bi_2O_3, $SrCO_3$, TiO_2, V_2O_5), and KCl salt were ground using mortar agate for 1 hour. Acetone was added to homogenize the sample and then the mixture was calcined at 780, and 820°C for 8 hours, respectively. Samples were washed with hot distilled water to diminish the remaining KCl salt. $AgNO_3$ test was conducted to identify the salt content of KCl. Finally, the free salt sample was dried using an oven at 80°C for 2 hours [30].

The sample products were characterized using (a) *X*-ray diffraction (XRD) instrument (Rigaku Miniflex diffractometer, Japan) with Cu Kα = 1.54059 radiation in the range measurement 2θ = 3-90° to obtain the structural character, (b) scanning electron microscope (Jeol JSM-6510, Japan) to obtain the morphology image of particle, and (c) ultraviolet-visible diffuse reflectance spectroscopy (UV-Vis DRS) instrument (Thermo Scientific Evolution 220 spectrometer, USA) to get the reflectance spectra, and the measurement were conduct from 200-800 nm wavelength.

The diffractogram samples were indexed to the standard data of $SrBi_4Ti_4O_{15}$ (database diffractogram of the Inorganic Crystal Structure Database (ICSD) No. 51863) and it was continued with the refinement process using Le-Bail method in Rietica software. The spectra reflectance samples were processed using the following Kubelka-Munk equation to determine the bandgap energy of samples (equation 1).

$$F(R) = \frac{(1-R)^2}{2R} = \frac{K}{S} \tag{1}$$

where $F(R)$ is the Kubelka-Munk factor, K is the molar absorption coefficient, S is the scattering coefficient, and R is the reflectance of an infinitely thick specimen.

The value of the band gap energy was determined from the plot between the photon energies (hv) (*x*-axis) and $(F(R).hv)^{1/2}$ (*y*-axis). The band gap energy was calculated by linear regression at the value of x (hv = band gap energy) when $y = 0$ [31].

3. Results and Discussion

Figure 1 shows the diffractogram of $SrBi_4Ti_{4-n}V_nO_{15}$ (n= 0, 0.05, 0.1, and 0.15) and it matched with the standard data of $SrBi_4Ti_4O_{15}$ (ICSD No. 51863). It can be seen that there was no new peak indicating the absence of an impurity phase that possibly was produced by the presence of vanadium precursor. It indicated that V was able to partially replace the Ti cation. Furthermore, the diffractogram samples were refined using Le Bail Method. The plot of diffractogram refinement and the results data were summarized in Figure 2 and Table 2 respectively. R_p and R_{wp} values obtained below 10%, which indicated good conformity between the standard data (ICSD No. 51863) and the sample diffractogram [32]. Furthermore, the crystallite size of samples were measured using Debye-Scherrer equation as shown in equation 2.

$$D = \frac{K\lambda}{\beta \cos\theta} \tag{2}$$

where D is the crystallite size (nm), λ is the wavelength of *X*-ray radiation with Cu k-α (1.5406 nm), K is the Scherer constant (0.9), β is the full width half at a maximum of peak (radians), and θ is the diffraction angle [33, 34]. The $SrBi_4Ti_{4-n}V_nO_{15}$ crystallite size calculation used the most intensive/highest

diffraction peak of $(2\theta\ (^o) = 30.4)$, the results of which are tabulated in Table 1. It can be seen that the crystallite size value was different in which it correlated to the changes in lattice dimension as a results of V doped $Bi_4Ti_4O_{15}$. The crystallite size of sample $n= 0.05$ was the largest probably caused by its broadening peak diffraction.
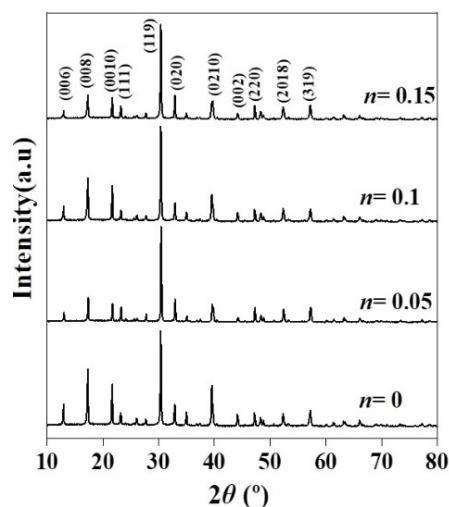
Fig 1. The diffractogram of $SrBi_4Ti_{4-n}V_nO_{15}$ ($n= 0, 0.05, 0.1,$ and 0.15)

Table 1. Crystallite size of $SrBi_4Ti_{4-n}V_nO_{15}$ ($n= 0, 0.05, 0.1,$ and 0.15)

V Dopant	Crystallite size (nm)
$n= 0$	55.25
$n= 0.05$	74.17
$n= 0.1$	58.38
$n= 0.15$	57.97
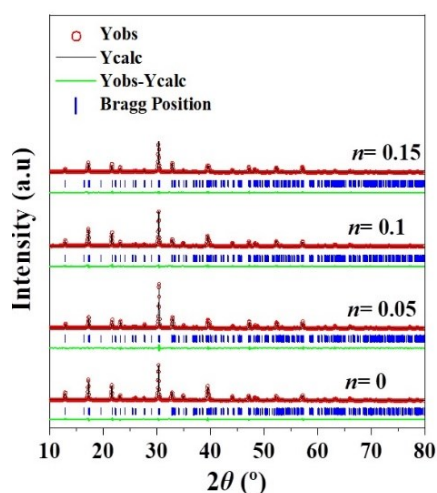
Fig 2. The refinement plot of $SrBi_4Ti_{4-n}V_nO_{15}$ ($n= 0, 0.05, 0.1,$ and 0.15) diffractogram

The refinement results (Table 2) exhibited that adding V dopants caused some changes in lattice parameters (a, b, and c). The cell volume slightly changed as a result of the relatively close value of ionic radii between V^{5+} and Ti^{4+} (ionic radii V^{5+} is 0.063 nm and Ti^{4+} is 0.068 nm) [9]. The decrease in lattice parameters, as well as cell volume at $n= 0.1$ and 0.15, was driven by the shortening of Ti-O bonds due to the substitution of V^{5+}, which had smaller ionic radii than Ti^{4+} [35]. Meanwhile, the increase of lattice parameter and cell volume at $n = 0.05$ was probably caused by a change in V valence, which induced

an oxygen vacancy, causing lattice contraction due to a sizeable electrostatic repulsion force on cation around the oxygen vacancy [36-38].

Table 2. Crystallographic data of the refinement result

Parameter	$SrBi_4Ti_{4-n}V_nO_{15}$			
	$n= 0$	$n= 0.05$	$n= 0.1$	$n= 0.15$
Crystal system	Orthorombic			
Space group	$A2_1am$			
Z	4	4	4	4
a (Å)	5.4491(8)	5.4530(3)	5.4460(9)	5.4458(3)
b (Å)	5.4340(8)	5.4387(2)	5.4376(8)	5.4311(4)
c (Å)	40.995(1)	41.003(2)	40.9801(2)	40.979(2)
Cell volume (Å³)	1213.9(3)	1216.0(1)	1213.6(3)	1212.0(1)
R_p (%)	9.76	9.90	9.46	9.33
R_{wp} (%)	8.76	8.83	9.13	8.55

Figure 3 shows the SEM micrograph and it can be seen that $SrBi_4Ti_{4-n}V_nO_{15}$ ($n= 0, 0.05, 0.1,$ and 0.15) had a slightly irregular shape at $n= 0$ but was dominated by a plate-like morphology. These results were in accordance with Chang et al. (2014) and Hao et al. (2007) stating that $SrBi_4Ti_4O_{15}$ had a plate-like morphology when synthesized by the molten salt method [25,39]. The formation mechanism of plate-like particles consists of two stages: the reaction stage and the particle growth stage. In the reaction stage, the precursors react with each other to form nuclei and at the growth stage, the nuclei are arranged to form a larger matrix with a plate-like shape [40,41]. The figure also exhibits that particle agglomeration decreases with the increasing concentration of V dopants because V-doping on Ti increases particle dispersion. As a result, it takes much energy for crystal growth to reduce the energy accumulated on the sample surface, resulting in a more stable state and decreased agglomeration [25,42-43]. It will give an advantage in photocatalysis applications because particles with low agglomeration can enhance photocatalytic activity due to increasing surface active sites [44]
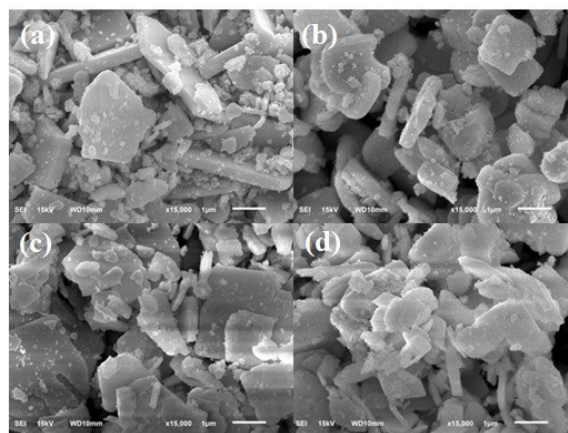
Fig.3. SEM micrographs of $SrBi_4Ti_{4-n}V_nO_{15}$: (a) $n= 0$; (b) $n= 0.05$, (c) $n= 0.1$, and (d) $n= 0.15$

Figure 4 shows the reflectance spectra of $SrBi_4Ti_{4-n}V_nO_{15}$ ($n= 0, 0.05, 0.1,$ and 0.15) and it can be seen that V dopant could

reveal light absorption at visible light wavelengths. Then, the data were calculated using the Kubelka-Munk equation [31]. Figure 5 and Table 3 depict the plot between $(F(R).hv)^{1/2}$ and the band gap energy (Tauc-plot), and the summary of band gap energy values respectively.

Table 3. The band gap energy values of $SrBi_4Ti_{4-n}V_nO_{15}$ ($n=$ 0, 0.05, 0.1, and 0.15)

Compound	Band gap energy (eV)
$SrBi_4Ti_4O_{15}$	3.04 (408 nm)
$SrBi_4Ti_{3.95}V_{0.05}O_{15}$	3.00 (413 nm)
$SrBi_4Ti_{3.90}V_{0.1}O_{15}$	2.86 (433 nm)
$SrBi_4Ti_{3.85}V_{0.15}O_{15}$	2.84 (436 nm)
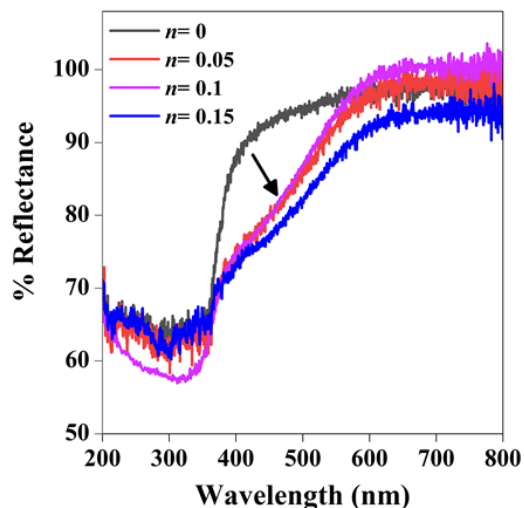
Fig. 4 The reflectance spectra of $SrBi_4Ti_{4-n}V_nO_{15}$ ($n=$ 0, 0.05, 0.1, and 0.15)
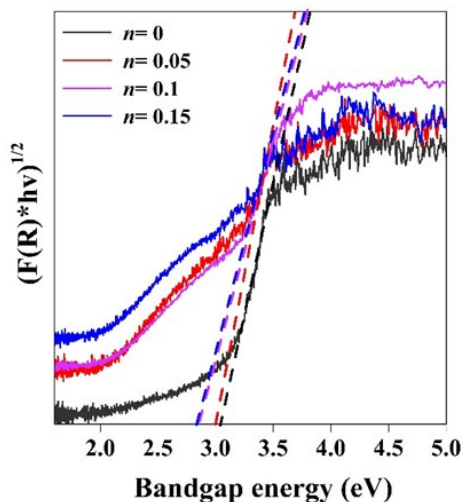
Fig 5. The Tauc-plot of $SrBi_4Ti_{4-n}V_nO_{15}$ ($n=$ 0, 0.05, 0.1, and 0.15)
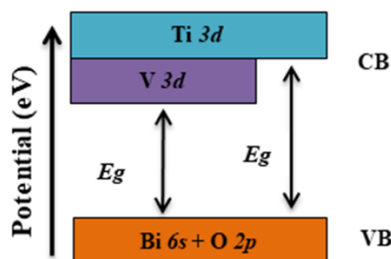
Fig 6. Illustration of band gap energy of V doped $SrBi_4Ti_4O_{15}$

The band gap energy values decreased with the increasing V dopant concentration. The conduction band consisted of Ti 3d, while the valence band consisted of Bi 6s and O 2p. The reduction of band gap energy value was related to new orbital revealing, i.e., V 3d by V dopant whose position was below the conduction band of $SrBi_4Ti_4O_{15}$. It was also caused by a mixture of d orbitals between Ti and V, causing a decrease in the position of the lower conduction band [45]. Dopant V could shift the Fermi level to the lower conduction band so that V 3d would assist in shifting the excited electrons by visible light irradiation [46]. The electronic structure of the V-doped $SrBi_4Ti_4O_{15}$ compound is proposed in Figure 6, adopting of V-doped $Bi_4Ti_3O_{12}$ model [15].

4. Conclusion

$SrBi_4Ti_{4-n}V_nO_{15}$ ($n=$ 0, 0.05, 0.1, and 0.15) was successfully synthesized using molten KCl salt. $SrBi_4Ti_{4-n}V_nO_{15}$ crystallized in space group $A2_1am$ and had a plate-like morphology. The band gap energy decreased linearly with an increase in vanadium dopant concentration due to the formation of a new electronic state by the V dopant. The band gap energy of $SrBi_4Ti_{4-n}V_nO_{15}$ ($n=$ 0, 0.05, 0.1, and 0.15) at range from 3.04 eV (408 nm) to 2.84 eV (436 nm) can give an advantage in photocatalyst application for being able to work in a broader light wavelength range. However, the photocatalyst activity experiment is required to further investigate the potency of V-doped $SrBi_4Ti_4O_{15}$ as photocatalyst compound.

References

1. R. Cao, H. Huang, N. Tian, Y. Zhang, Y. Guo and T. Zhang, *Novel Y doped Bi_2WO_6 photocatalyst: hydrothermal fabrication, characterization and enhanced visible-light-driven photocatalytic activity for rhodamine b degradation and photocurrent generation*, Mater. Charact., 101 (2015) 166–172.

2. J. Guo, L. Shi, J. Zhao, Y. Wang, K. Tang, W. Zhang, C. Xie and X. Yuan, *Enhanced visible-light photocatalytic activity of Bi_2MoO_6 nanoplates with heterogeneous $Bi_2MoO_{6-x}@Bi_2MoO_6$ core-shell structure*, Appl. Catal. B: Environ., 224 (2018) 692–704.

3. W. Wu, S. Liang, X. Wang, J. Bi, P. Liu and L. Wu, *Synthesis, structures and photocatalytic activities of microcrystalline $ABi_2Nb_2O_9$ (A= Sr, Ba) powders*, J Solid State Chem., 184 (2001) 81-88.

4. Z. Chen, H. Jiang, W. Jin, and C. Shi, *Enhanced photocatalytic performance over $Bi_4Ti_3O_{12}$ nanosheets with controllable size and exposed {001} facets for rhodamine b degradation*, Appl. Catal. B: Environ., 180 (2016) 698–706.

5. S. Tu, Y. Zhang, A. H. Reshak, S. Auluck, L. Ye, X. Han, T. Ma and H. Huang, (2018). *Ferroelectric polarization promoted bulk charge separation for highly efficient CO_2 photoreduction of $SrBi_4Ti_4O_{15}$*. Nano Energy, 56 (2018) 840–850.

6. A.A. Alemi, R. Kashfi and B. Shabani, *Preparation and characterization of novel Ln (Gd^{3+}, Ho^{3+} and Yb^{3+})-doped Bi_2MoO_6 with aurivillius layered structures and photocatalytic activities under visible light irradiation*, J Mol Catal A Chem., 392 (2014) 290–298.

7. R.Z. Hou and X.M. Chen, *La^{3+} substitution in four-layers Aurivillius phase $SrBi_4Ti_4O_{15}$*, Solid State Commun., 130 (2004) 469–472.

8. D. Do, S.S. Kim and J.W. Kim, *Effects of vanadium doping on structure and electrical properties of $SrBi_4Ti_4O_{15}$ thin films*, Appl. Surf. Sci., 255

(2009) 4531–4535.

9. G.N. Shao, S.M. Imran, S.J. Jeon, S.J. Kang, S.M. Haider and H.T. Kim, *Sol–gel synthesis of vanadium doped titania: effect of the synthetic routes and investigation of their photocatalytic properties in the presence of natural sunlight*, Appl. Surf. Sci., 351 (2015) 1213-1223.

10. T. Wang and T. Xu, *Effects of vanadium doping on microstructures and optical properties of TiO₂*, Ceram. Int., 43 (2016) 1558–1564.

11. X. Ma, L. Xue, S. Yin, M. Yang and Y. Yan, *Preparation of V-doped TiO₂ photocatalysts by the solution combustion method and their visible light photocatalysis activities*, J. Wuhan Univ. Technol. Mater. Sci. Ed., 29 (2014) 863–868.

12. R. Handayani, W. Safitri, N Aini, A. Hardian and A. Prasetyo, *Synthesis and characterization of vanadium doped Bi₄Ti₃O₁₂ as photocatalyst material,* IOP Conf. Ser. Mater. Sci. Eng., 578 (2019) 1, 1-5.

13. T. Kamegawa, J. Sonoda, K. Sugimura, K. Mori and H. Yamashita, *Degradation of isobutanol diluted in water visible light sensitive vanadium doped TiO₂ photocatalyst*, J. Alloys Compd., 486 (2009) 685-688.

14. H. Bantawal, S.U Shenoy and K.D. Bhat, *Vanadium-doped SrTiO₃ nanocubes: insight into role of vanadium in improving the photocatalytic activity*, Appl. Surf. Sci., 513 (2020) 145858.

15. D. Gu, Y. Qin, Y. Wen, T. Li, L. Qin and H.J. Seo, *Electronic structure and optical properties of V-Doped Bi₄Ti₃O₁₂ nanoparticles*, J. Alloys Compd., 695 (2017) 2224-2231.

16. J. Zhu, X.Y. Mao and X.B. Chen, *Properties of vanadium-doped SrBi₄Ti₄O₁₅ ferroelectric ceramics,* Solid State Commun., 130 (2004) 363–366.

17. A.S. Rini, A. Nabilla and Y. Rati, *Microwave-assisted biosynthesis and characterization of ZnO film for photocatalytic application in methylene blue degradation*, Commun. Sci. Technol., 6(2) (2021) 69–73.

18. K. Wu, H.L. Tan, C. Zhang, Z. Teng, Z. Liu, Y.H. Ng, Q. Zhang and C. Su, *Recent advances in two-dimensional ultrathin Bi-based photocatalysts*, Prog. Mater. Sci., (2022) 101047.

19. A.P. Jakhade, M.V. Biware and R.C. Chikate, *Two-dimensional Bi₂WO₆ nanosheets as a robust catalyst toward photocyclization*, ACS Omega, 2 (2017) 7219–7229.

20. W. Jiang, T. Chen, X. Yang, L. Ruan, Y. Liu, X. Meng, G. Xu and G. Han, *Surfactant free synthesis of single crystalline Bi₄Ti₃O₁₂ nanosheets with excellent visible light photocatalytic activity*, Catal. Surv. Asia, 23 (2019) 322-331.

21. T. Cheng, X. Sun, T. Xian, Z. Yi, R. Li, X. Wang and H. Yang, *Tert-Butylamine/Oleic Acid-assisted morphology tailoring of hierarchical Bi₄Ti₃O₁₂ architectures and their application for photodegradation of simulated dye wastewater.* Opt. Mater., 112 (2021) 110781.

22. N. Sreeram, V. Aruna, R. Koutavarapu, D.Y. Lee and J. Shim, *Visible-light-driven indium vanadium oxide nanosheets supported bismuth tungsten oxide nanoflakes heterostructure as an efficient photocatalyst for the tetracycline degradation*, Chemosphere, 229 (2022) 134477.

23. X. Wen, C. He, B. Wu, X. Huang, Z. Huang, Z. Yin, Y. Liu, M. Fang, X. Wu and X. Min, *Molten salt synthesis, growth mechanism, and photoluminescence of rod chlorapatite microcrystallites.* CrystEngComm., 21 (2019) 11 1809–1817.

24. T. Kimura, *Molten salt synthesis of ceramic powders. Advances in Ceramics-Synthesis and Characterization, Processing and Specific Applications.* London, UK. Intechopen, 2011.

25. Y. Chang, J. Wu, B. Yang, S. Zhang, T. Lv and W. Cao, *Synthesis and properties of high aspect ratio SrBi₄Ti₄O₁₅ microplatelets.* Mater. Lett., 129 (2014) 4 12–15.

26. S.K Gupta and Y. Mao (2021). *Recent developments on molten salt synthesis of inorganic nanomaterials: A Review.* J. Phys. Chem. A, 125

27. D.R. Novianti, F. Haikal, U.A. Rouf, A. Hardian and A. Prasetyo, *Synthesis and characterization of Fe-doped CaTiO₃ polyhedra prepared by molten NaCl salt*, Indones. J. Sci. Technol., 7 (2022) 1 17-21.

28. W. Zhao, Z. Jia, E. Lei, L. Wang, Z. Li and Y. Dai, *Photocatalytic degradation efficacy of Bi₄Ti₃O₁₂ micro-scale platelets over methylene blue under visible light*, J. Phys. Chem. Solids, 74 (2013) 11 1604-1607.

29. H. He, J. Yin, Y. Li, Y. Zhang, H. Qiu, J. Xu, T. Xu and C. Wang, *Size controllable synthesis of single-crystal ferroelectric Bi₄Ti₃O₁₂ nanosheet dominated with {001} facets toward enhanced visible-light-driven photocatalytic activities.* Appl. Catal. B., 156-157 (2014) 35-43.

30. S.N. Himmah, P. Sari and A. Prasetyo, *Characterization of vanadium-doped BaBi₄Ti₄O₁₅ prepared by molten KCl salt method*, JKPK., 7 (2022) 1 1-11.

31. P. Makula, M. Pacia and W. Macyk. *How to correctly determine the band gap energy of modified semiconductor photocatalysts based on UV–Vis spectra*, J. Phys. Chem. Lett., 9 (2018) 23 6814-6817.

32. B.H. Toby, *R factors in Rietveld analysis: How good is good enough?*, Powder Diffr., 21 (2006) 1 68-70.

33. L. Alexander and H.P. Klug, *Determination of crystallite size with the X-Ray spectrometer*, J. Appl. Phys., 21 (1950) 137.

34. E.M. Benali, A. Benali, M. Bejar, E. Dhahri, M.P.F. Graca, M.A. Valente and B.F.O. Costa, *Effect of synthesis route on structural, morphological, Raman, dielectric, and electric properties of La₀.₈Ba₀.₁Bi₀.₁FeO₃*, J Mater Sci: Mater Electron, 31 (2020) 3197-3214.

35. R.D. Shannon, *Revised effective ionic radii and systematic studies of interatomic distances in halides and chalcogenides*, Acta Crystallogr. A, A32 (1976) 751-767.

36. E.V. Ramana, N.V. Prasad, D.M. Tobaldi, J. Zavasnik, M.K. Singh, M.J. Hortiguela, M.P. Seabra, G. Prasad and M.A. Valente, *Effect of samarium and vanadium co-doping on structure, ferroelectric and photocatalytic properties of bismuth titanate,* RSC Adv., 7 (2017) 9680-9692.

37. D.P. Dutta and A.K. Tyagi, *Facile sonochemical synthesis of Ag modified Bi₄Ti₃O₁₂ nanoparticles with enhanced photocatalytic activity under visible light*, Mater. Res. Bull., 74 (2016) 397-407.

38. D. Marrocchelli, S.R. Bishop, H.L. Tuller and B. Yildiz, *Understanding chemical expansion in non-stoichiometric oxides: ceria and zirconia case studies*, Adv. Funct. Mater., 22 (2012) 1958-1965.

39. H. Hao, H. Liu, Y. Liu, M. Cao and S. Ouyang, *lead free SrBi₄Ti₄O₁₅ and Bi₄Ti₃O₁₂ material fabrication using the microwave-assisted molten salt synthesis method*, J Am. Ceram. Soc. 90 (2007) 5 1659-1662.

40. Z. Zhao, X. Li, H. Ji and M. Deng, (2014). *Formation mechanism of plate-like Bi₄Ti₃O₁₂ particles in molten salt fluxes*, Integr. Ferroelectr. 154 (2014) 1 154-158.

41. S.D. Marella, N. Aini, A. Hardian, V. Suendo and A. Prasetyo, (2021). *The effect of synthesis temperature on the plate-like particle of Bi₄Ti₃O₁₂ obtained by molten NaCl salt method,* J. Pure Appl. Chem., 10 (2021) 1 64-71.

42. J. Wang, X. Ye, X. Yaer, Y. Wu and B. Zhang, *Key to enhance thermoelectric performance by controlling crystal size of strontium titanate*, Mod. Phys. Lett. B., 29 (2015) 1550167

43. R. Ebrahimi, A. Malei, A. Rezaee, H. Daraei, M. Safari, G. McKay, S. Lee and A. Jafari, *Synthesis and application of Fe-doped TiO₂ nanoparticles for photodegradation of 2,4-D from aqueous solution*, Arab. J. Sci. Eng,. 46 (2020) 6409-6422.

44. A.A. Isari, A. Payan, M. Fattahi, S. Jorfi and B. Kakavandi, *Photocatalytic degradation of rhodamine b and real textile wastewater using Fe-doped TiO₂ anchored on reduced graphene oxide (Fe-TiO₂/rGO): characterization and feasibility, mechanism and pathway*

studies, Appl. Surf. Sci,. 462 (2018) 549-564.

45. A. Kubacka, A. Fuerte, A. Matinez-Arias and M. Fernandez-Garcia, *Nanosized Ti-V mixed oxides: effect of doping level in the photo-catalytic degradation of toluene using sunlight-type excitation,* Appl. Catal. B:

Environ., 74 (2007) 1-2 26-33.

46. M. Khan, Y. Song, N. Chen and W. Cao, *Effect of V doping concentration on the electronic structure, optical and photocatalytic properties of nano-sized V-doped anatase TiO$_2$*, Mater. Chem. Phys., 142 (2013) 1 148-153.